ICONE-4

International Conference on Nuclear Engineering
Volume 1 — Part B
ASME 1996

STEAM-WATER TWO-PHASE FLOW IN LARGE DIAMETER VERTICAL PIPING AT HIGH PRESSURES AND TEMPERATURES

Hisham A. Hasanein
University of Toronto
Toronto, Ontario, Canada

Albert M. C. Chan
Ontario Hydro Technologies
Toronto, Ontario, Canada

Masahiro Kawaji
University of Toronto
Toronto, Ontario, Canada

Yuzuru Yoshioka
Japan Atomic Power Company
Chiyoda-Ku, Tokyo 100, Japan.

ABSTRACT

Experimental data on steam-water two-phase flow in a large diameter (20", 50.08 cm I.D.) vertical pipe at elevated pressures and temperatures (2.8MPa/230°C - 6.4MPa/280°C) have been obtained. Void fraction, two-phase mass flux, phase and velocity distributions as well as pressure drop along the test pipe have been measured using the Ontario Hydro Technologies (OHT) Pump Test Loop.

The void fraction distributions were found to be axially symmetric and nearly flat over a wide range of two-phase flow conditions. The two-phase flow regime could be inferred from the dynamic void fluctuations data. For the 280 °C tests, the flow was found to be relatively stable with bubbly flow at low average void fractions and churn turbulent or wispy-annular flow at higher void fractions. At 230 °C, the flow became rather oscillatory and slugging was suspected at relatively low voids. It has also been found that the average void fractions in the test section can be determined reasonably accurately using the axial pressure drop data.

NOMENCLATURE

A = area (m^2)
DP6 = axial pressure drop from differential pressure transducer #6 (kPa)
DP7 = axial pressure drop from differential pressure transducer #7 (kPa)
G = mass flux (kg/m^2s)
g = gravitational acceleration (m/s^2)
h = distance between two axial pressure transducers (m)
J = momentum exchange factor {see Equation (2)}
N = attenuated gamma flux ($\#/cm^2s$)
P = pressure (MPa)
u = velocity (m/s)

Greek Symbols

α = void fraction
$\overline{\alpha}$ = average void fraction
ΔP = pressure drop (kPa)
ρ = density (kg/m^3)

Subscripts

av = average
c = core region of the test pipe
cw = region between the core and wall regions
ΔP_f = axial pressure drop
f = saturated water
g = saturated steam
γD = gamma densitometer
j = local (j=1 to 5)
T = total
w = wall region of the test pipe

C/OE41

INTRODUCTION

No information on steam/water two-phase flow behavior in large diameter pipes (10" or larger) at elevated pressures is available in the open literature. However, there are many applications, in the nuclear, chemical and petroleum industries among others where two-phase flows in large diameter pipes at elevated pressures and temperatures are encountered routinely or under accident scenarios.

In the nuclear industry the next generation of reactors emphasizes the elimination of active safety systems and introduction of passive components in order to improve reliability and safety. The Simplified Boiling Water Reactor (SBWR), currently under development by the General Electric (GE) in the US in collaboration with the Japan Atomic Power Company (JAPC) among others is an example of such reactors. In the SBWR, natural circulation is adopted for core cooling and the total core flow depends on the net driving head between the downcomer and the chimney. The void fraction and void distribution in the chimney thus exert a strong influence on the total core flow. Since there are no two-phase flow data for the large chimney (about 6 m in diameter), a divided chimney is proposed in the SBWR to avoid the complex multi-dimensional two-phase flow behavior. The large circular chimney is subdivided into smaller square chimneys (or grids) each of 0.9mX0.9m in size. This size was chosen for easy access to the fuel assembly while maintaining a fully developed flow distribution within each grid region (Shiralkar et al, 1992). However, no reliable steam-water data exist even for the smaller grids in the partitioned chimney. The data are important from design and safety point of view.

The objective of the current work is to obtain reliable experimental data on steam-water two-phase flow parameters in a 24" diameter pipe (61.0 cm O.D., 50.8 cm I.D.) at elevated pressures and temperatures. Void fractions, two-phase mass fluxes, phase and velocity distributions as well as pressure drop measurements in two-phase vertical up-flow have been made. The local void fractions and velocities were measured using a multi-detector gamma densitometer and a five tap Pitometer, respectively. By combining the two sets of measurements, the two-phase mass flux could be obtained.

DESCRIPTION OF TEST FACILITY

The Ontario Hydro Technologies (OHT) Pump Test Loop with a full-scale CANDU reactor pump was used to perform the study. The pump was a vertical, single suction and double volute centrifugal pump. The configuration of the OHT Test Loop is shown schematically in Figure 1 and specifications of the pump are given by Chan et al (1995). The loop has three parallel, vertical inverted-U branches, connecting the suction and discharge headers. Each branch features a flow control valve and a venturi flow-meter. The loop branches were fabricated using 24" (61.0 cm O.D., 50.8 cm I.D.) carbon steel pipes and the suction and discharge headers were made out of 36" (91.4 cm O.D.) carbon steel pipes. The height of all the branches was about 12 m which represents a length-to-diameter ratio of about 24. The loop is designed for operations up to 9.4 MPa and 280 °C in pressure and temperature, respectively.

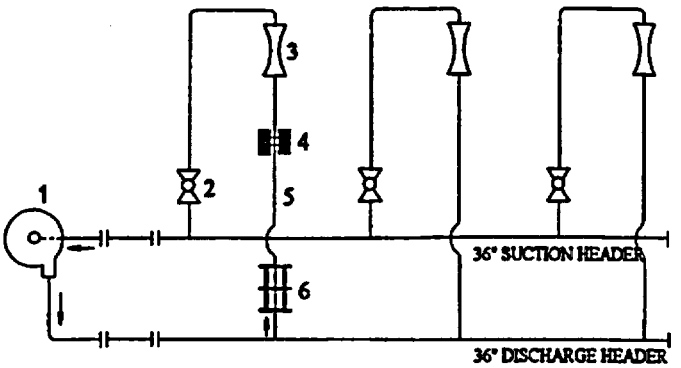

1- Pump (Bruce NGS 'A' Pump)

2- Flow Control Valve

3- Universal Venturi Tube

4- Gamma Densitometer and Five Tap Pitometer

5- 24" Carbon Steel Pipe (12 m in length)

6- Perforated S.S. Plate Type Flow Straightening Vane

Figure 1: Schematic of the test facility

Details of the Test Section

The test section is the riser of the branch closest to the pump. Figure 2 shows a schematic of the test section and the instruments involved. The test section is a 12.4 meters long, 24" (50.8 cm I.D.) carbon steel pipe. The riser features a perforated stainless steel plate type flow straigtener located inside the pipe at about 2.0 meters from its inlet above the discharge header and a venturi-meter near the top of the pipe. The flow through the test section could be controlled using a flow control valve located at the downcomer of the branch. A specially designed multi-detector gamma densitometer and a five-tap Pitometer for local void fraction and velocity heads measurements were located at about 7.2 meters from the riser inlet. Pressure and differential pressure transducers were also installed to measure the pressure drop along the length of the test section.

Instrumentation

The test loop was extensively instrumented with a full compliment of transmitters used to cover the process conditions of the flow loop. They included pump and motor parameters, pressure and differential pressures along the test section, void fraction, and void and velocity distributions at about mid-height of the test section. These instruments are described below in more detail.

Multi-detector Gamma Densitometer

Figure 3 shows a schematic of the gamma densitometer used in the present study. This gamma densitometer was specially designed to measure void fraction and phase distributions in large diameter, thick-walled steel pipes.

010042

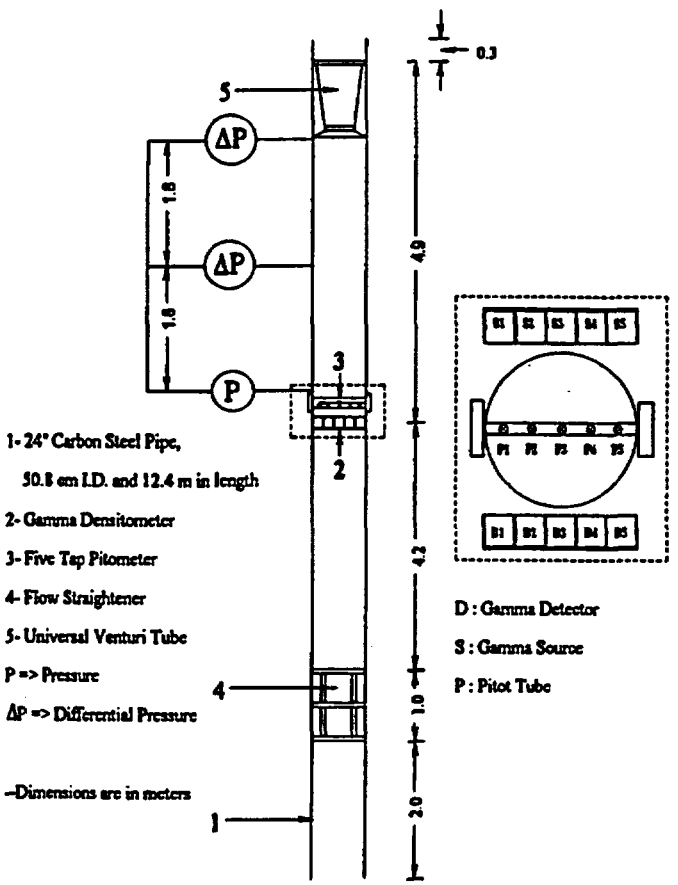

Figure 2: Schematic of the test section

A Cesium-137 gamma source with a principal photon energy of 0.662 MeV was used. The 10-Curie Cs-137 line source supplied by the 3M Electrical Specialties Division had a diameter of 12.7 mm and an active length of 508 mm. Lead collimators with four internal partitions were provided on both sides of the pipe to define the beam cross-section and to divide the pipe into five sections for *chordal-average* void fraction measurements. Lead partitions (19 mm thick and 406 mm long on each side of the pipe) were used to reduce cross-talk or interference from other beams. Transmitted gamma fluxes were measured using five 102mmX102mm NaI(T1) scintillation detectors (101.6 mm square) that have a high detection efficiency (close to 100%) and relatively good energy resolution. The latter property was particularly important for the present study because of the large number of scattered gammas present. Good energy resolution makes it possible to discriminate against the lower energy scattered gammas for better measurement accuracy.

In order to minimize system noises and obtain more stable output signals, a pulse-counting signal processing system was used. The system consisted of a pre-amplifier, a linear amplifier, a single channel pulse height analyzer, a scaler for digital output and a ratemeter for analog output.

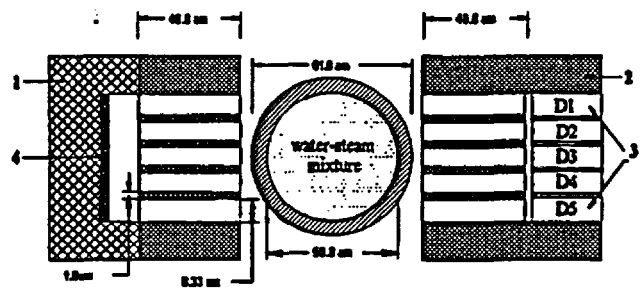

1- Sheilding Cask (12.7 cm Lead)

2- Lead Collimator

3- D1->D5: NaI(T1) Scintillators (10.16 cm X 10.16 cm X 5.08 cm)

4- Cesium-137 Gamma Source (10 Ci)

Figure 3: Schematic of the multi-detector gamma densitometer

The system could count and process individual gamma pulses from the scintillator. Energy discrimination was achieved by a single-channel analyzer which could be set to band-pass the gamma energies of interest.

The gamma densitometer was placed on a platform supported by hangers. The platform was fixed to the test section so that possible loop vibration under two-phase flow conditions would not affect the gamma densitometer measurements. Details of gamma densitometer platform are given by Chan et al.(1995).

The void fraction was determined from the attenuated gamma intensities using the following expression,

$$\alpha_j = \frac{\ln\left[N(\alpha_j)/N(0)\right]}{\ln\left[N(1)/N(0)\right]}, \qquad (1)$$

where :

$N(\alpha_j)$ = attenuated gamma intensity for a given void fraction α_j in the test pipe,

$N(0)$ = attenuated gamma intensity when the test pipe is filled with liquid only, and

$N(\alpha)$ = attenuated gamma intensity when the test pipe is filled with vapor only.

Five chordal-average void fraction measurements (α_j where j = 1 to 5) were thus obtained using Equation (1).

The OHT multi-detector gamma densitometer was calibrated statically using a piece of pipe identical to the test pipe and air\water at room temperature. In the calibration, the pipe was closed at the bottom and "simulators" of different shapes and sizes were used to simulate the different void and flow patterns. Details of the static calibration were described by Chan et al. (1992). It was found that the measured void fractions compared very well with the actual void fractions in the test pipe with a maximum deviation of about 5% void. The ability of the multi-detector gamma densitometer to identify phase distributions

010043

for different cross-section average void fractions was also demonstrated by Chan et al (1992).

. Five Tap Pitometer (Annubar)

Design details of the annubar are shown in Figure 4. The annubar was made out of 1.5" (38.1mm) pipe (XXH A106 GR B) with eight 1/8"(3.2mm) diameter holes drilled into the pipe diametrically along its length as shown in Figure 4.

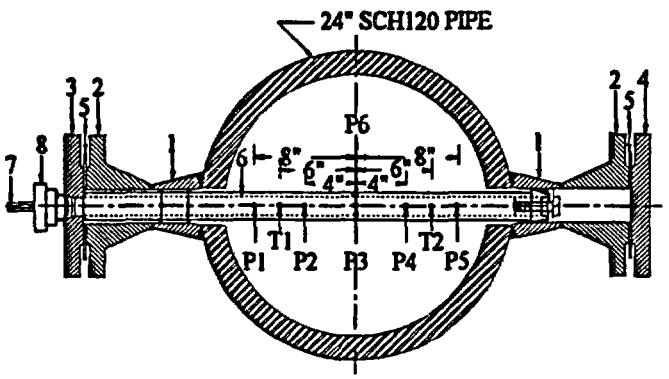

Figure 4: Details of the five tap pitometer

Six 1/8"(3.2mm) tubes were silver soldered to six of these holes. Five of the holes were made facing the flow forming an array of five Pitot tubes. The remaining hole at the middle perpendicular to the others was used as the static pressure tap. Two 1/8"(3.2mm)T-type (Copper-Constantan) stainless steel-sheathed, grounded junction thermocouples were fed through the two remaining holes for temperature measurements. The thermocouples were silver-soldered to the end of the two holes. The tubing as well as the thermocouples were then led out through blind flanges using CONAX multiple tube gland.

Five Celesco differential pressure transducers (Model DP 30) were connected to the stainless steel tubes to measure the velocity heads for the five Pitot tubes. The transducers had a range of 0 to 34 kPa and were bled regularly to ensure that the connecting lines were free from vapor bubbles.

The dynamic head in two-phase flows is given by (Anderson et al., 1960),

$$\Delta P = \frac{1}{2}\left[\alpha\rho_g u_g^2 + J(1-\alpha)\rho_f u_f^2\right], \qquad (2)$$

where;

α = local void fraction,

ρ_g = steam density,

ρ_f = water density,

u_g = local steam velocity,

u_f = local water velocity and

J = a momentum exchange factor ranging in value from 1 to 2 and being a strong function of the void fraction as discussed by Reiman et al. (1984).

In the present analysis, J was assumed to have a constant value of 1.0. The local dynamic pressure heads as measured by the Pitometer can thus be written as;

$$\Delta P_j = \frac{1}{2}\left[\alpha_j\rho_g u_{g,j}^2 + (1-\alpha_j)\rho_f u_{f,j}^2\right], \qquad (3)$$

where j takes the values from 1 to 5.

Assuming no slip between the two phases (i.e. $u_f = u_g$), the local mass flux can be given by

$$G_j = \sqrt{\left(2\Delta P_j\left[\alpha_j\rho_g + (1-\alpha_j)\rho_f\right]\right)}. \qquad (4)$$

where ΔP_j and α_j are measured using the Pitometer and multi-detector gamma densitometer, respectively. The total mass flux is obtained from the local mass fluxes using the following expressions,

$$G_T = \frac{\sum_{j=1}^{5} G_j A_j}{A_T} \qquad (5)$$

and

$$A_T = \sum_{j=1}^{5} A_j, \qquad (6)$$

where A_T is the total flow area of the test pipe while A_j is the cross-section area of the local pipe segment associated with measuring volume j.

The methodology used to measure two-phase mass fluxes was verified both in vertical and horizontal two-phase flows using 4" SCH 80 pipes. Detailed descriptions of the calibration loops can be found from Chan (1990). In both loop configurations, good agreement (within 15%) between the measured and actual total two-phase mass fluxes was obtained.

.Axial Pressure Pressure Drop Measurements

Two Celesco differential pressure transducers (Model DP 30) were used to measure the pressure drop along the length of the test section above the Pitometer as shown in Figure 2. The transducers had the same range as those used in the annubar (i.e. 0-34 kPa).

The axial pressure drop measurements were also used to deduce the average void fraction in the test section assuming the axial acceleration and friction pressure drops were negligible. The average void fraction, $\bar{\alpha}_{\Delta h}$, can thus be expressed as:

$$\bar{\alpha}_{\Delta h} = \frac{\rho_f}{\rho_f - \rho_g} - \frac{\Delta P_t}{(\rho_f - \rho_g)gh}, \qquad (7)$$

where :

ΔP_t = pressure drop along the length of the test section

C/CC44

g = gravititational acceleration and

h = the distance over which the pressure drop was measured.

The average void fraction as obtained from Equation (7) can be compared with the average void fraction measured directly by the multi-detector gamma densitometer using the following expression:

$$\bar{\alpha}_{,o} = \frac{\sum_{j=1}^{5} \alpha_j A_j}{A_T} \quad (8)$$

where $\bar{\alpha}_{,o}$ is the average void fraction obtained from the gamma densitometer measurements.

. Data Acquisition System

A PC based-data logger was used for data acquisition. Signals from a total of nineteen transducers were acquired at a rate of 20 Hz during the tests. The parameters measured included the total pressure and temperature in the test section, discharge pressure and temperature, dynamic heads from the Annubar Pitot tubes, axial pressure drops, local void fractions, and pump head. Data acquisition and analysis were performed using the commercially available software package VIEWDAC.

TEST CONDITIONS AND PROCEDURE

The nominal operating conditions in the test loop were controlled by heat addition from the pump and heat removal by an air-cooled heat exchanger attached to the loop. During the heat-up phase in preparation for the tests, the heat exchanger was valved off so that the test loop could be heated up from room temperature to 280 °C in about two and half hours. After the test loop attained the desired temperature, a flow through the heat exchanger was established to maintain the loop temperature constant. The flow through the heat exchanger was adjusted continually during the test as the pump motor power dropped off under two-phase flow operation. Typically, the loop temperature could be held to within 5 °C of the desired value.

Two-phase flow in the test loop was created by draining water from the loop into a storage tank. The void fraction in the test section was monitored by the gamma densitometer during the tests. Draining was interrupted several times to maintain a constant void fraction in the test section. The flow through the test section could then be varied by adjusting the flow control valve in the test section slowly and in steps. Three test section void fractions at 25%, 50% and 75% were attempted during the tests to study the effect of varying mass flowrates on two-phase flow behaviour in the test pipe. However, for the lower temperature (230 °C) tests, the pump stopped pumping and the flow in the test section dropped to zero at the intermediate void fraction of about 50% when the flow in the test section was reduced progressively by closing the flow control valve. Therefore, test data were obtained only in the lower void range for the 230 °C tests. The two-phase mass flux in the test section was varied from about 500 to 2000 kg/m²s in both cases.

Since the two-phase flow conditions in the test loop and the test section were varied slowly, it may be assumed that quasi-steady state conditions prevailed during the test and useful two-phase flow test data could also be obtained when the loop was being drained.

The test procedure also provided in-situ calibration for the gamma densitometer in each test. At the beginning of the test, full pipe conditions with water at the test temperature were obtained for all the five detectors. Empty pipe conditions with steam at the same test temperature were obtained at the end of the test. Uncertainties in void fraction measurements could thus be reduced significantly.

RESULTS AND DISCUSSION

Since the test results for different tests at the same nominal temperature were found to be very similar, only two tests, one at each temperature, were analyzed and discussed in the study reported here.

Transient Test Data

. Void Fraction

The transient average void fraction in the test pipe for the two temperature conditions are shown in Figures 5 and 6, respectively. The test data shown here have been averaged over 3.6 seconds to reduce fluctuations. The actual test data can be found from Chan et al. (1995). The average void fractions were obtained from the five local void fraction measurements by using Equation (8). It can be seen that no void was detected in the test section for a significant length of time into the test, due to condensation of steam in the pump impeller at low pump suction voids. Noghrehkar, et al.(1995) found that for suction void fractions below about

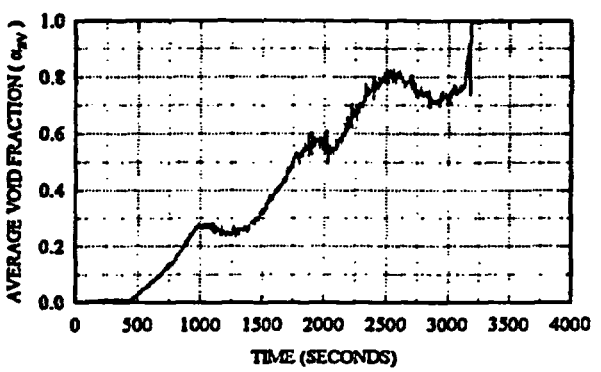

Figure 5: Average void fraction at a nominal temperature of 280 °C

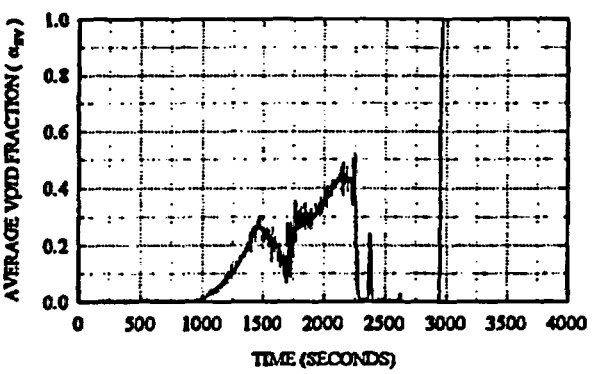

Figure 6: Average void fraction at a nominal temperature of 230 °C

C/CC95

15%, all the steam condenses in the pump and no voids appear in the pump discharge header to which the test section was connected. After the initial period, the steam void in the test section increased steadily. Draining was stopped at a few void levels to vary the flow rate in the test section by changing the position of the flow control valve as described in the Test Procedure.

For the higher temperature test (280 °C), three void levels at about 25%, 55% and 80% were used (Figure 5). It was found that the void fraction in the test section remained nearly constant when the flow rate in the test section was reduced at the two lower void levels. At the 80% void level, the average void fraction in the test section decreased significantly when the flow rate was varied. This effect was more pronounced for the 230 °C tests (Figure 6). The observed void versus flow characteristics in the test section could be resulted from the two-phase pump behaviour and the test loop configuration. At high loop voids, the pump head will be highly degraded, an increase in the flow resistance in the test section due to closing of the flow control valve can have a major impact on the distribution of the two-phase flow to the three branches including the test section from the discharge header (Figure 1). In fact, in the lower temperature (230 °C) tests, the pump stopped circulating the water when the flow to the test section was severely restricted (using the control valve connected to the test section) at high void levels (Figure 6). The water in the test section then drained back down and formed a water column in the lower half of the test section suspended by the little pump head still available. The average void fraction then became zero until the pump was shut down and the water in the test section could drain to the header. An empty pipe condition was then detected.

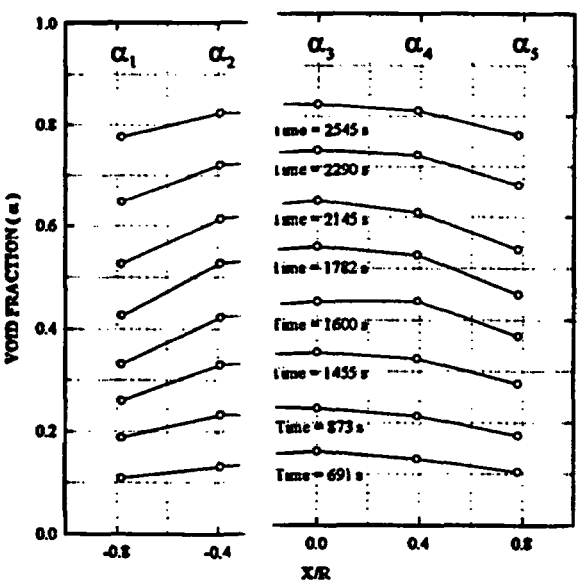

Figure 7: Void fraction distribution at a nominal temperature of 280 °C

The five transient local void fraction measurements were obtained as described previously. The void distributions across the diameter of the test pipe were plotted at different times during the transients as shown in Figures 7 and 8 for the high and lower temperature tests, respectively. In both cases, the two local void fraction measurements close to the pipe walls, α_1 and α_5, are nearly equal and are lower than the void fractions in the middle of the pipe, α_2, α_3 and α_4. Maximum differences of about 9% void for the 280 °C test and about 13% for the 230 °C test were found. It can also be seen that α_2, α_3 and α_4 are very close to each other. However, since the counts from GD#2, GD#3 and GD#4 are affected by the low void region near the wall, the test section cross section was divided into three concentric regions as shown schematically in Figure 9.

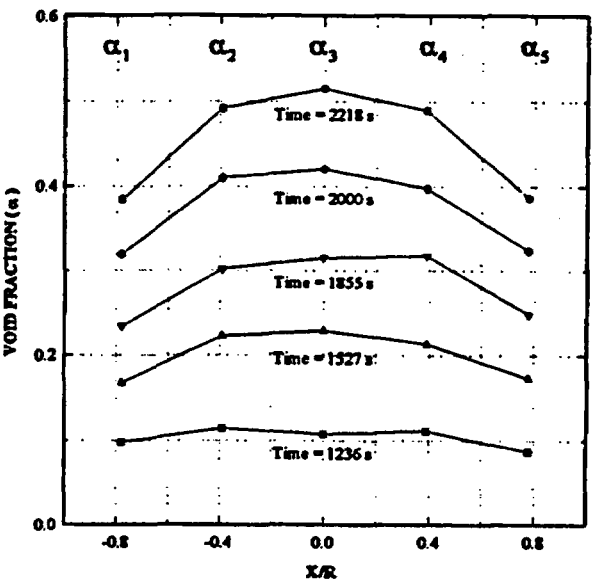

Figure 8: Void fraction Distribution at a nominal temperature of 230 °C

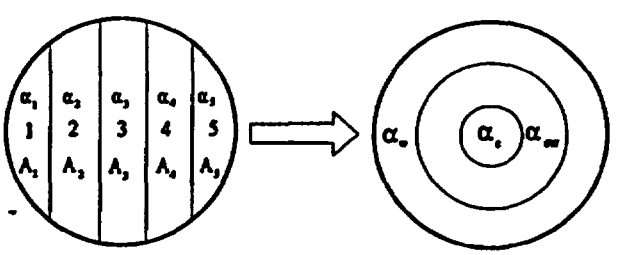

Figure 9: Geometric Transformation

C/CC46

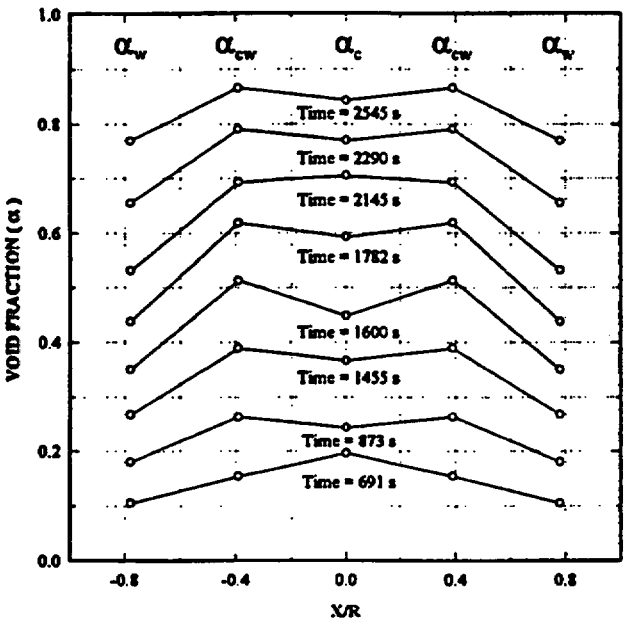

Figure 10: Void fraction distribution at a nominal temperature of 280 °C

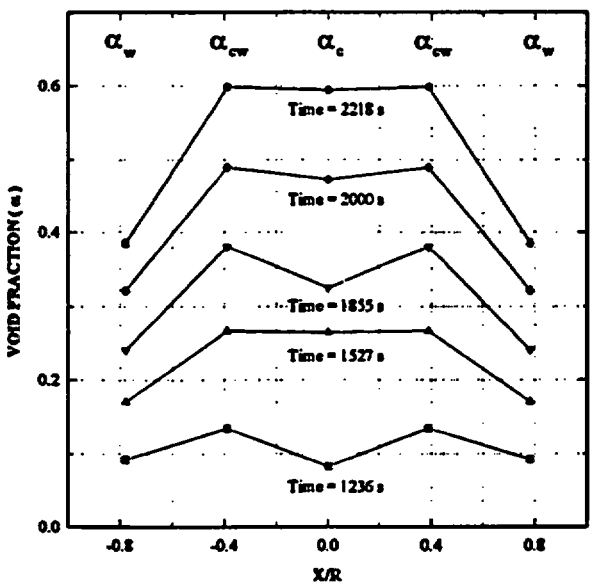

Figure 11: Void fraction distribution at a nominal temperature of 230 °C

A simple geometrical transformation was then employed in order to obtain the wall void fraction α_w and the core void fraction α_c and the void fraction for the region in between α_{cw}. The results are shown in Figures 10 and 11 for the high and lower temperature tests, respectively. Maximum difference of about 15% void and 22% void were found between the core and the wall regions for the 280 °C and 230 °C tests, respectively.

. Mass Fluxes

The transient total mass fluxes in the test section are shown in Figures 12 and 13 respectively for the 280 ° and 230 °C tests. Again, the test data shown have been averaged over 3.6 seconds to reduce fluctuations. The actual test data can be found in Chan et al.(1995). The local mass fluxes were obtained once by employing $\alpha_1,.., \alpha_5$ in Equation 4 and another by employing α_c , α_{cw} and α_w in the same equation. The average and maximum relative deviations of the corresponding values obtained using the two procedures were found to be negligible at about 0.65 % and 1.7 %, respectively.

It can be seen that the mass fluxes decreased steadily as the loop void increased due to pump head degradation under two-phase flow operations. The range of mass fluxes of interest was found to vary between 500 and 2000 kg/m^{2}s when a substantial amount of void was present in the test pipe. The dips in the total mass fluxes resulted from slow closing and opening of the flow control valve in the test section at given void levels.

The flow distributions across the diameter of the test pipe are plotted in Figures 14 and 15, respectively for the two test conditions at different times during the transients.

The single-phase water flow profiles were also obtained at time zero. It was found that the single-phase flow profiles were skewed with much higher mass fluxes in the "outer" region of the test pipe for both cases.

This flow asymmetry is most probably due to the entrance effects at the test pipe inlet as the flow enters the vertical riser from the horizontal header as shown schematically in Figure 16.

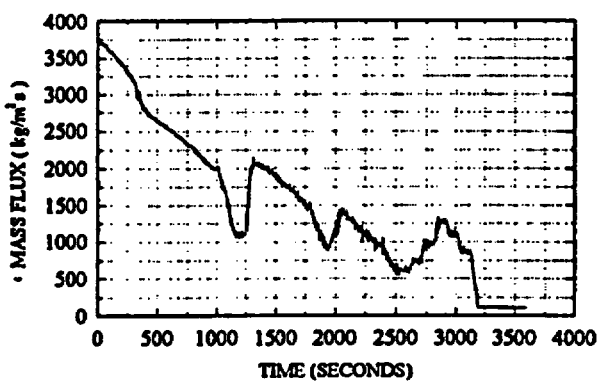

Figure 12: Total mass flux at a nominal temperaturte of 280 °C

C/CC47

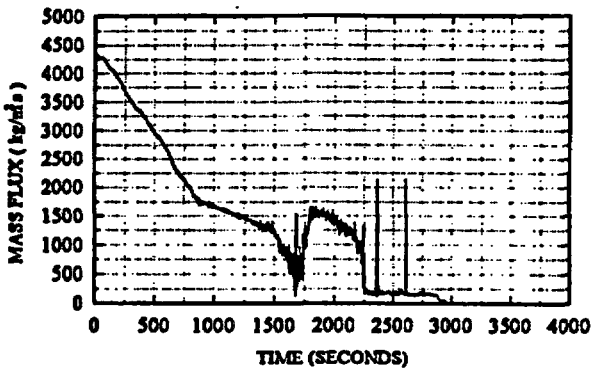

Figure 13: Total mass flux at a nominal temperaturte of 230 °C

The fluid particles moving toward the outer wall of the test pipe would move faster than the fluid particles moving close to the inner wall of the pipe due to the centrifugal acceleration. This behavior is commonly observed in branching flows (Seeger et al.(1986), Popp et al.(1983), Lahey et al.(1990) and Lamonnier et al.(1991)). The flow profiles, however, became less assymmetric as time progressed and higher void fractions existed in the test pipe. This is expected since the presence of

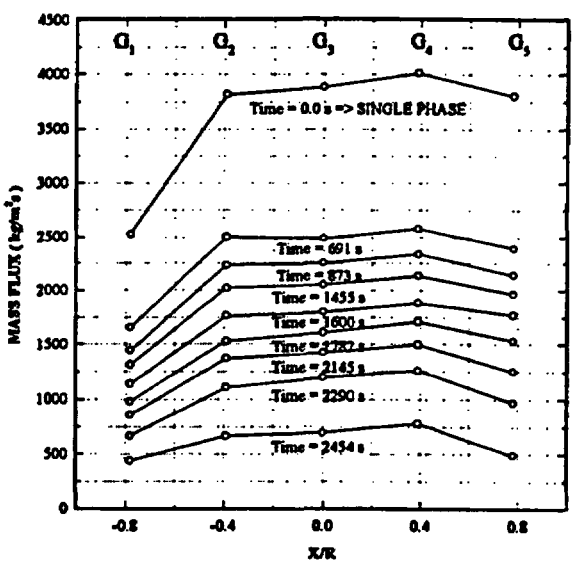

Figure 14: Local Mass Flux Distribution at a Nominal Temperature of 280 °C

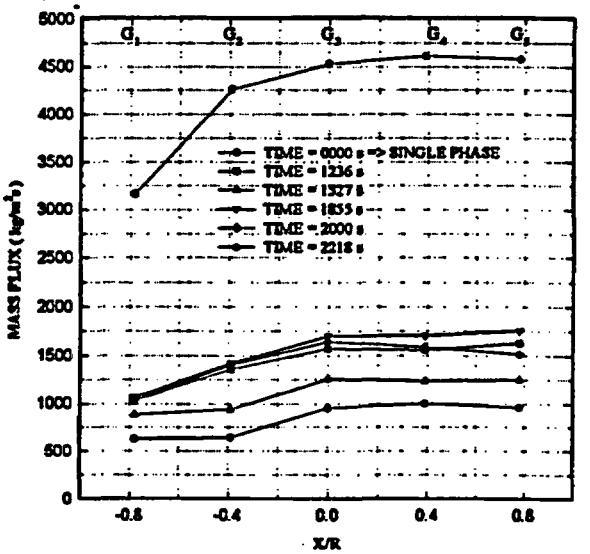

Figure 15: Local mass flux distribution at a nominal temperature of 230 °C

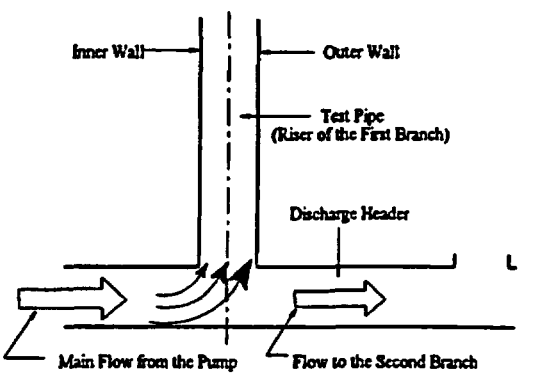

Figure 16: Flow Orientation at the Test Pipe Inlet

steam voids in the test pipe would enhance turbulence and promote radial mixing which consequently would result in flattening of the velocity profile. This is especially true for the 280 °C test as shown in Figure 14. However, the effect of test pipe void fraction on the flow profile was less evident in the 230 °C test as shown in Figure 15 due to the lower maximum void fraction attained in the test.

. Axial Pressure Drops

Pressure drop along the test section was measured at two locations downstream of the Pitometer and gamma densitometer as dipicted in Figure 2. Actual transient test data for both DP6 and DP7 are given by Chan et al.(1995) for the two test conditions considered. They are reduced

CICC 4-8

and compared here in Figure 17 for the 280 °C test. It can be seen that the two measurements behaved essentially in the same manner as expected. Since the frictional and acceleration pressure drops are negligible in the present tests, DP6 and DP7 can be used to calculate the average void fraction in the test section as described previously.

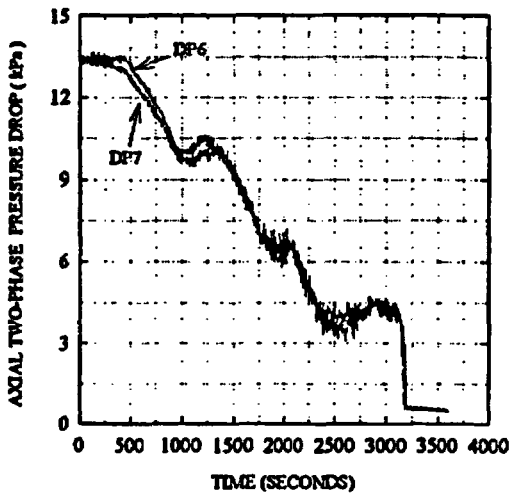

Figure 17: Axial Pressure Drops at a Nomina Temperature of 280 °C

The average void fractions in the test section calculated from the axial pressure drop measurements, $\overline{\alpha}_{\Delta p}$, were compared with the corresponding values obtained using the gamma densitometer, $\overline{\alpha}_{\gamma D}$, as shown in Figures 18 and 19, respectively for the two temperature conditions investigated. Good agreement was obtained in both cases.

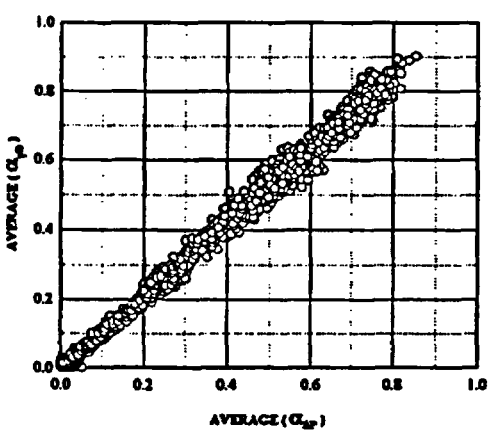

Figure 18: Average void fractions ($\alpha_{\gamma D}$) versus average void fractions ($\alpha_{\Delta P}$) at a nominal temperature of 280 °C

The average deviations of $\overline{\alpha}_{\Delta p}$ from $\overline{\alpha}_{\gamma D}$ were found to be 6.1% for the 280 °C test and 18% at 230 °C indicating greater discrepancy between the two void fractions. In general, the average void fractions based on pressure drop measurements were found to be slightly lower than the gamma densitometer measurements in both cases. This is due to the fact that the acceleration and frictional pressure drops were ignored in the hydrostatic head calculations. The differences tend to increase as void increases. It should also be noted that greater data scatter in the lower temperature (230 °C) case (Figure 19) indicates that the two-phase flow is more oscillatory.

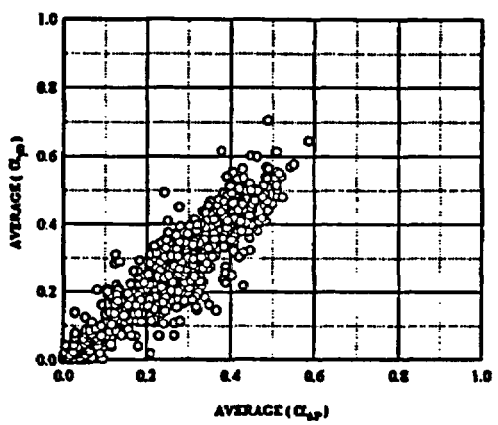

Figure 19: Average void fractions ($\alpha_{\gamma D}$) versus average void fractions ($\alpha_{\Delta P}$) at a nominal temperature of 230 °C

Dynamic Local Void Fluctuations

The potential for using the dynamic local void fluctuations to identify two-phase flow regimes in the test section was investigated. Preliminary observations are presented below.

The local void fluctuations at different average voids for the 280 °C test are shown in Figure 20. Only α_1, α_2 and α_3 are shown because of symmetry. Time periods of 20 seconds are shown in the figure. The void fluctuations were acquired at a frequency of 20 Hz.

In general, all three local void measurements show a similar pattern of fluctuations for all given average void fractions. At lower voids, the fluctuations tend to be fairly uniform and have relatively low amplitude and high frequency. This means that the flow regime is most likely bubbly flow. At higher voids, the void fluctuations show a distinct lower frequency component with large density variations. This may indicate the breakdown of homogeneous bubbly flow and the formation of regions with high bubble density or even gas slugs followed by regions with low bubble density or liquid slugs. With a further increase in average void fractions, the fluctuations are dominated more by the low frequency oscillations representative of annular flow. It may be speculated that the flow regime is approaching churn or wispy-annular flows.

The dynamic void fluctuations for the lower temperature (230 °C) test are shown in Figure 21 for two different void levels. It can be seen that even at relatively low average voids, the fluctuations are dominated by low frequency and high amplitude oscillations. The fluctuations

C1CC49

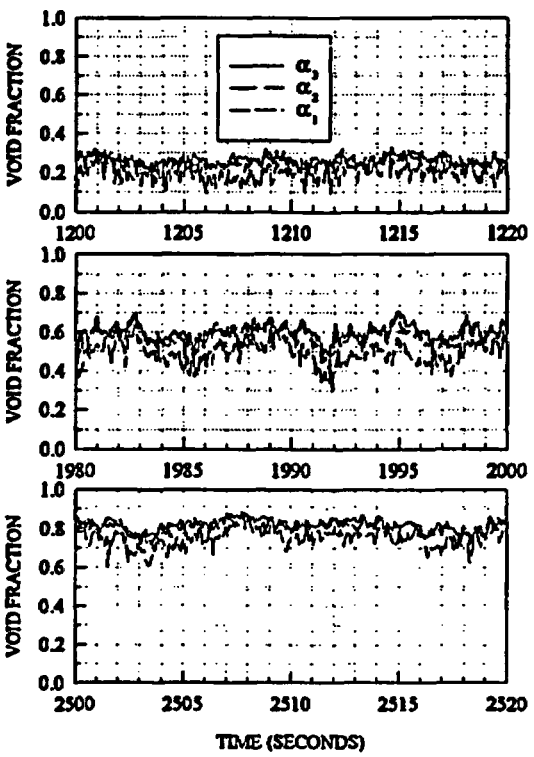

Figure 20: Void fraction fluctuations at 280 °C

increased significantly at higher voids. This strongly suggests that the flow was highly unstable and slugging might be occuring in the test pipe. It is also interesting to note that the oscillations are essentially in phase for all five local void measurements at the higher void level. This may imply that large water or steam slugs with diameters close to the diameter of the test pipe are passing through at regular intervals. However, it is very difficult from this information alone to conclude that slug flow as traditionally defined in literature existed. Some evidences from air-water experiments at atmospheric pressure in large diameter pipes seem to support the non-existence of slug flow in large diameter pipes. Larson (1987) indicated that slug flow was not materialised in a 30.5-cm vertical pipe and instead, a transition from bubbly to bubbly-churn flow with strong local recirculation patterns took place. Hashemi et al.(1986) concluded that for the 30.5-cm pipe tests, slug flow was not observed and rather the flow regime progressed from bubbly to a churn-type flow with the presence of large bubbles of about 15-cm in diameter. Ohnuki et al.(1995) did not recognise air slugs which occupied the flow path in a 48-cm vertical pipe with L/D of 4.2. This behaviour may be explained following the theory developed by Kocamustafaogullari et al.(1984). The theory is based on the hypothesis that the breakup of fluid particles will take place when the rate of growth of a disturbance at the interface between the dispersed and continuous phases is faster than the rate at which it propagates around that interface. This implies that there are situations where bubbles can not coalesce to form slugs that are as large as the pipe dimeter and consequently slug flow formation is prevented.

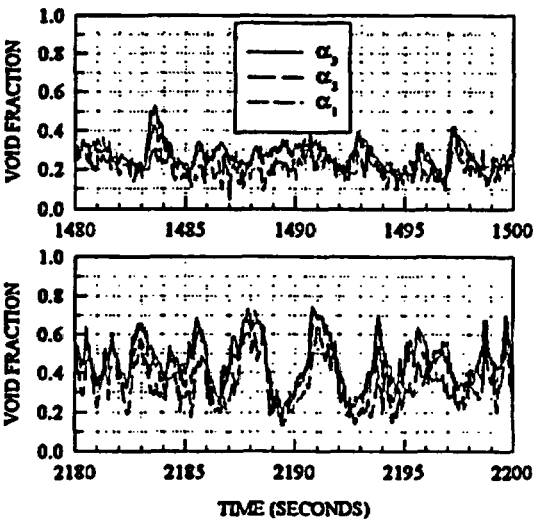

Figure 21: Void fraction fluctuations at 230 °C

CONCLUDING REMARKS

Based on the preliminary analysis of the test results obtained, the following conclusions can be drawn.

1. At a nominal temperature of 280 °C, the average void fraction in the test section reached 80% and the two-phase mass flux could be controlled in steps from 500 to 1400 kg/m^{2}s at the highest void level. The void range was more restricted for the lower temperature case, and the maximum average void fraction attained was for the 230 °C tests was about 50%.
2. High quality two-phase flow test data in a large diameter vertical pipe were obtained. The void fraction distributions were found to be symmetrical with respect to the pipe axis and the void profile was relatively flat across the diameter of the pipe over a wide range of two-phase flow conditions.
3. The flow profiles were found to be skewed across the diameter of the test pipe with higher mass fluxes in the "outer" region of the pipe. The flow profile, however, became less assymmetric as void was created and increased in the test pipe. This may be attributed to the increased turbulence and radial mixing provided by the presence of steam bubbles.
4. Average void fractions calculated from the axial pressure drop data were found to be in good agreement with those obtained using the gamma densitometer.
5. The two-phase flow regime in the test pipe may be inferred from the dynamic void fluctuations. For the 280 °C tests, bubbly flow was considered to exist at low void fractions. At higher void fractions, there were indications that the flow may become churn turbulent or wispy-annular. For the lower temperature (230 °C) tests, there were indications that large slugs might have existed even at relatively low voids, but this needs to be further confirmed.
6. The two-phase flow in the test pipe was relatively stable for the higher temperature (280 °C) tests. However, it was rather oscillatory at lower temperatures (230 °C).

ACKNOWLEDGMENTS

The authors would like to acknowledge participation of Dr. B.S. Shiralkar and Dr. V. Arik of the General Electric Company in the present project.

REFERENCES

Anderson, G.H. and Mantzouranis, B.G., 1960, "Two-phase (Gas/Liquid) Flow Phenomena - Part II Liquid Entrainment," *Chem. Engrg. Sci.* Vol. 12, pp. 233-242.

Chan,A.M.C., Hasanein, H.A. and Kawaji, M., 1995, "Basic Study on Two-Phase (steam-water) flow in Large Diameter Vertical Piping," Final Contract Report, Submitted to Japan Atomic Power Company (JAPC), Japan.

Chan, A.M.C., 1992, "Void Fraction Measurements in Large Diameter Pipes with Thick Metal Walls or Complex Internal Geometries," *Proceedings of the National Heat Transfer Conference.* American Nuclear Society, pp. 236-244.

Chan, A.M.C. and Bzovey, D., 1990, "Measurement of Mass Flux in High Temperature High Pressure Steam-water Two-Phase Flow using a combination of Pitot Tubes and a Gamma Densitometer," *Journal of Nuclear Engineering and Design*, Vol. 122, pp. 95-104.

Hashemi, A., Munis, A. and Goodman, J., 1986, "Two-Phase Flow Regimes and Carry-Over in a Large-Diameter Model of a PWR Hot Leg," EPRI NP-4530Project 2393-2, Final Report.

Kocamustafaogullari, G., Chen, I. Y. and Ishii, M., 1984, "Unified Theory for Predicting Maximum fluid Particle size for Drops and Bubbles," NUREG/CR-4028, ANL-84-67.

Lahey, Jr., R. T., 1990, "The Analysis of Phase Seperation and Phase Distribution Phenomena using Two-Fluid Models," *Nuclear Engineering and Design*, Vol. 122, 1990, pp. 17-40.

Lamonnier, H. and Herview, E., 1991, "Theoretical Modelling and Experimental Investigation of Single-Phase and Two-Phase Flow Division in a Tee-Junction," *Nuclear Engineering and Design*, Vol. 125, pp. 201-213.

Larson, T. K., 1987, "An Investigation of Integral Facility Scaling and Data Relation Methods (Integral System Test Program)," NUREG/CR-4531, EGG-2440, pp. 43.

Noghrehkar, G.R., Kawaji, M., Chan, A.M.C.,Nakamura, N. and Kukita, Y.,1995, "Investigation of Centrifugal Pump Performance Under Two-Phase Flow Conditions," *Journal of Fluids Engineering*, Vol. 117, pp. 129-137.

Ohnuki, A. Akimoto, H. and Sudo, Y., 1995, "Flow Pattern and Its Transition in Gas-Liquid Two-Phase Flow along a Large Vertical Pipe," *Proceedings of the 2nd International Conference on Multiphase Flow*, Kyoto, Japan, pp. FT1-17.

Popp, M. and Sallet, D. W., 1983, "Experimental Investigation of One- and Two-Phase flow through a Tee Junction," *Proceedings of the Int. Conference on the Physical Modelling of Multi-Phase Flow*, Coventry, England, pp. 67-88.

Reiman, J., Kusterer, H. and John, H., 1984, "Two-phase Mass Flow Rate Measurements with Pitot Tubes and Density Measurements, Measuring Techniques in Gas-Liquid Two-phase Flows," Springer, Berlin-Heidelberg, pp. 625-650.

Seeger, W., Reimann, J. and *Müller*, U., 1986, "Two-Phase Flow in a *T*-Junction with a Horizontal Inlet," PART I: Phase Separation. *Int. J. Multiphase Flow* Vol. 12, No. 4, pp. 575-585.

Shiralkar, B.S., Alamgir, Md. and Andersen, J.G.M., 1992, "Thermal Hydraulic Aspects of the SBWR Design," *Proceedings of the Int. Conference on Design and Safety of Advanced Nuclear Power Plants*, Tokyo, Japan, Vol. III, pp. 31.1-1 -31.1-

010051